

Cross sections for deuterium, tritium, and helium production in $\bar{p}p$ collisions at $\sqrt{s}=1.8$ TeV

T. Alexopoulos,⁷ E. W. Anderson,³ N. N. Biswas,^{4,*} A. Bujak,⁵ D. D. Carmony,⁵ A. R. Erwin,⁷ C. Findeisen,⁷ A. T. Goshaw,¹ K. Gulbrandsen,⁷ L. J. Gutay,⁵ A. S. Hirsch,⁵ C. Hojvat,² J. R. Jennings,⁷ V. P. Kenney,⁴ C. S. Lindsey,⁶ J. M. LoSecco,⁴ N. Morgan,⁸ K. Nelson,⁹ S. H. Oh,¹ N. Porile,⁵ L. Preston,⁵ R. Scharenberg,⁵ B. Stringfellow,⁵ M. Thompson,⁷ F. Turkot,² W. D. Walker,¹ C. H. Wang,¹ and J. Warchol⁴

(Fermilab E735 Collaboration)

¹Duke University, Durham, North Carolina 27708

²Fermi National Accelerator Laboratory, Batavia, Illinois 60510

³Iowa State University, Ames, Iowa 50011

⁴University of Notre Dame, Notre Dame, Indiana 46556

⁵Purdue University, W. Lafayette, Indiana 47907

⁶Royal Institute of Technology, Frescativ 10405, Stockholm, Sweden

⁷University of Wisconsin, Madison, Wisconsin 53706

⁸Virginia Polytechnic Institute and State University, Blacksburg, Virginia 24061

⁹University of Virginia, Charlottesville, Virginia 22901

(Received 10 February 2000; published 8 September 2000)

We present the results of a search for the production of light elements in $\bar{p}p$ collisions at the Fermilab Tevatron collider. Momentum, time of flight, and dE/dx measurements are used to distinguish nuclei from elementary particles. A production ratio for deuterium to hydrogen is calculated and compared to the primordial value of the big bang model. Some evidence for tritium is found and none for helium isotopes.

PACS number(s): 13.60.Hb, 13.60.Le, 13.60.Rj

I. INTRODUCTION

The production of deuterons has been observed in many elementary particle collisions. The early production of antideuterons in 30 GeV p -Be collisions [1] made it clear that the mechanism was not a simple pickup of existing nucleons or a spallation process. The deuteron momentum spectrum was consistent with the product of the observed momentum spectra for the independent constituents. This feature is now incorporated in a successful coalescence model [2] that works well for describing the production of nuclei even in heavy ion collisions. Deuteron production is not limited to hadron collisions. Antideuterons have been observed in e^+e^- interactions at center of mass energies as low as 10 GeV [3], which suggests that the production mechanism needs to be understood at the parton level.

The very appearance of nuclei in elementary particle collisions seems to present a puzzle. Temperatures in multiparticle production are typically 150–200 MeV, whereas nuclear binding energies are only about 8 MeV per nucleon for light nuclei. Nuclei could potentially originate from a process other than the primary collision, such as the decay of a massive elementary particle or the hadronization of a quark.

II. EXPERIMENTAL SETUP

This experiment was performed in the C0 intersection of the Fermilab $\bar{p}p$ collider. The floor plan of the spectrometer is shown in Fig. 1. A general description of the various components can be found in other publications [4]. We will

briefly describe here those features which directly affect this analysis.

Mass determinations depended critically on the performance of the time of flight system. Upstream and downstream scintillators produced timing signals t_u and t_d made

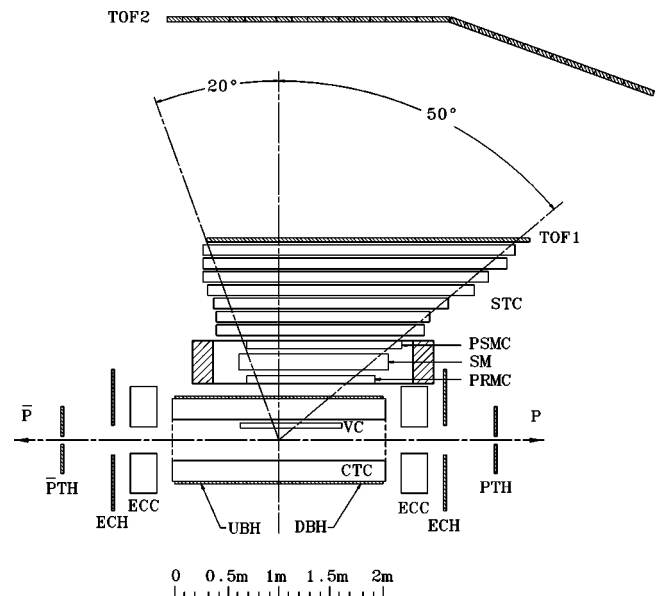


FIG. 1. Plan view of E735 detector. $\bar{P}TH$ =antiproton trigger hodoscope, ECH= end cap hodoscope, ECC=end cap chambers, UBH= upstream barrel hodoscope, DBH=downstream barrel hodoscope, PTH= proton trigger hodoscope, CTC=central tracking chamber, VC=vertex chamber, PRMC=pre magnet chamber, SM=spectrometer magnet, PSMC=post magnet chamber, STC=straw tube chambers, TOF1=time of flight #1 hodoscope, TOF2=time of flight #2 hodoscope.

*Deceased.

by the earliest arriving particles from the interaction. The difference in arrival time of these two signals, $t_u - t_d$, was used to calculate a z coordinate for the interaction vertex position by assuming that the earliest arriving particles close to the beam line travel at the speed of light. The average of the upstream and downstream times yielded an interaction time that was independent of vertex position, $t_0 = (t_u + t_d)/2$.

The interaction z coordinate obtained from $t_u - t_d$ was required to agree with the z coordinate of a vertex obtained from the intersection of tracks found in three drift chamber planes (VC in Fig. 1) pressed against the beam pipe. In turn, a *spectrometer track* was required to have three hits in these drift planes and to originate from the interaction point determined by the timing and the intersection of the other tracks. This greatly reduced the possibility that nuclei in the spectrometer were the result of unrelated beam collisions with the wall of the vacuum pipe.

Two planes of scintillators, TOF1 and TOF2, in the spectrometer arm gave timing signals t_1 and t_2 as particles from the interaction passed through them. The velocity of particles could be calculated using any of the time differences $t_{01} = t_1 - t_0$, $t_{02} = t_2 - t_0$, and $t_{12} = t_2 - t_1$. To improve the accuracy of the timing measurements, it was necessary to make an empirical time-walk correction based on the amplitude of the timing pulse as recorded by an analog to digital converter (ADC). The time of flight (TOF) system is described in more detail elsewhere [5].

III. MASS MEASUREMENTS

The momenta of charged particles in the spectrometer arm were determined by tracking them through the inhomogeneous magnetic field with a fourth order Runge-Kutta integration. The momentum measurement for each particle was used with t_{02} to make the most accurate mass calculation, m_2 . Two other mass calculations, m_1 and m_{12} , were also made using the remaining flight times with the same momentum measurement.

By fitting the observed variation of mass resolution for pions, kaons, and protons as a function of momentum, we determined that the rms uncertainty for the time of flight measurement was 170 ps. The mass uncertainty was fit to the form

$$\Delta m^2 = 2m^2 \sqrt{(ap)^2 + (b/\beta)^2 + g^2 \gamma^4}, \quad (1)$$

where p is the particle momentum, β is the velocity of the particle relative to the speed of light, and $\gamma = 1/\sqrt{1 - \beta^2}$. The value of g is the average fractional timing error $g = \Delta t/t$. The values of a , b , and g were determined in a simultaneous fit to three particle masses using TOF1 and TOF2. The fit results for TOF1 are the curves shown in Fig. 2. This parametrization of the measuring errors was subsequently used to estimate the expected widths for measurements of heavier particles.

IV. ΔE MEASUREMENTS

The scintillation material used in the TOF1 and TOF2 hodoscopes was 2-in.-thick Bicron BC-408. The thickness

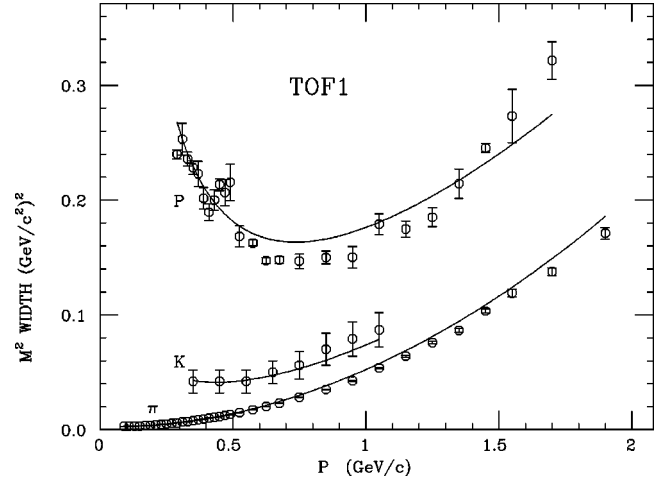


FIG. 2. Data points are rms variations of mass measurements as a function of momentum. Curves are a global fit to the error formula given in the text.

was chosen to provide an adequate number of photoelectrons for the required time resolution. The large number of photoelectrons also ensured good pulse height resolution.

For phototubes on the TOF1 hodoscope, both the anode pulse height and the dynode 9 pulse height were recorded. This permitted off-line corrections for pulse height non-linearity caused by the high gain operating conditions used for the Amperex XP2020 phototube. The corrections were applied on a pulse by pulse basis. Pulse height was not monitored for dynode 9 on the TOF2 counters, so a less accurate average correction for non-linearity was made based on a study of the pulse height versus momentum data for slow protons.

At the outset of the experiment it was anticipated that the ADC information would be used only for time-walk corrections, so that the range of the ADC was not set to cover a wide variation in particle energy loss. In a number of cases a 2.5 times minimum ionizing track which hit scintillator near a light pipe would overflow the ADC range for the phototube on that light pipe. Fortunately each end of a scintillator is viewed by a separate phototube. For the present study we have taken our energy loss measurements from the phototube located at the greater distance from the position at which the particle passed through the scintillator. We have thus traded the statistical accuracy in pulse height measurement for the extended range provided by light absorption in the scintillator. In this way all ADC's can measure the energy loss ΔE up to a value at least 6 times that of minimum ionization without ADC range overflow.

Because there was considerable absorption of light in the scintillator itself, light from each hodoscope element was fit to two attenuation lengths using data from minimum ionizing pions. With the use of these attenuation lengths the observed pulse heights were then corrected for absorption according to the point from which light originated. Often this point of origin was determined from both the tracking program and the time difference between phototubes on opposite ends of the scintillator. No events were used in this experiment if both light origins did not agree with each other within errors.

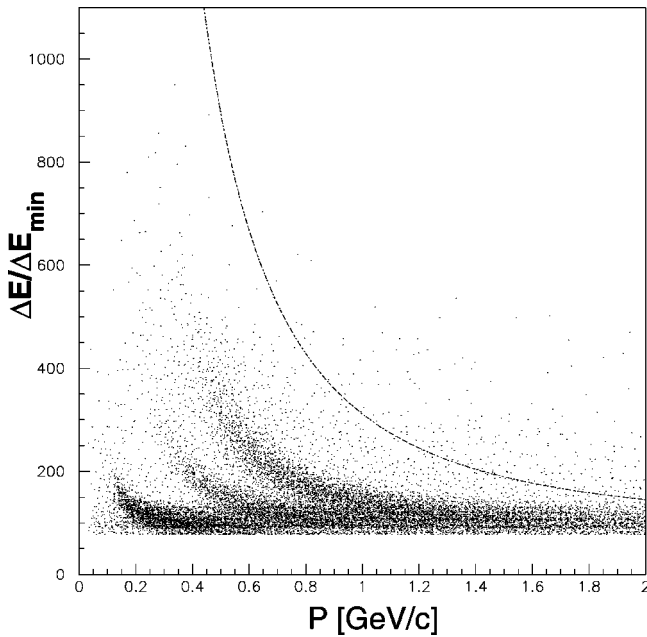


FIG. 3. Ratio of energy loss in TOF2 to energy loss of a minimum ionizing pion in the same scintillator. The dashed curve indicates the expected location of deuteron points uncorrected for scintillator saturation.

In addition, ΔE measurements were not used if the tracking indicated the presence of another track in the same scintillator or in either of the adjacent scintillators. Corrections were made later for the loss of these tracks in higher multiplicity events.

Figure 3 shows a scatter plot of relative $\Delta E/\Delta E_{min}$ versus momentum of particles, where ΔE_{min} is the energy loss observed in the scintillator for pions at a momentum corresponding to minimum dE/dx . Cuts have been made on the data plotted here to ensure that the tracks came from a single consistent vertex identified both by the tracking and the upstream and downstream time of flight counters. It is possible to identify bands in the plot that correspond to pions, kaons, and protons. The sharp edge in ΔE along the bottom edge of the scatter plot is an artifact due to a threshold.

V. EVIDENCE FOR DEUTERON PRODUCTION

The dashed curve in Fig. 3 is a simple estimate of where a band might lie for deuterons. It is uncorrected for saturation effects in the scintillator. One can see that the signal must be small and perhaps obscured by a background of false measurements. To reduce the background a cut was made using the fact that dE/dx for particles with unit electron charge is very nearly a universal function for all particles with the same mass over momentum ratio. All tracks which do not follow this function closely should be eliminated from mass plots as potential mismeasured tracks. Figures 4(a) and 4(b) are mass plots made using such a cut. In addition ΔE was required to be greater than 2.5 times minimum. The mass plotted is the average of m_1 and m_2 so that only particles with momentum high enough to reach TOF2 are included in Fig. 4. There is some possible deuteron signal

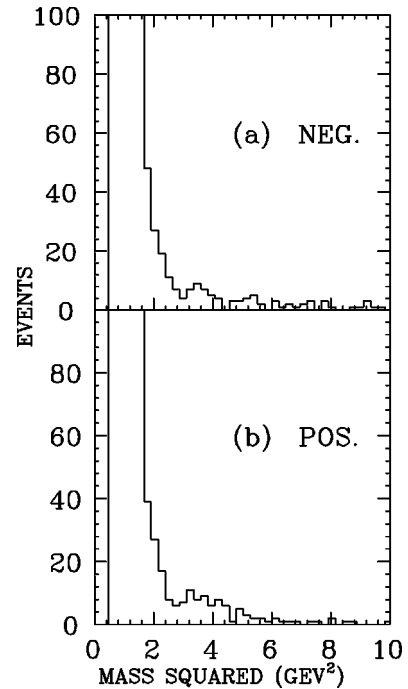


FIG. 4. Average of the mass squared values using TOF1 and TOF2 for (a) negative and (b) positive particles.

above the background around a mass squared of 3.5 GeV/c², perhaps 17 d^- events and 27 d^+ events. Events in these plots carry unit weight and are not corrected by their prescaled trigger factors [6]. In the analysis that follows we will use other cuts in the presence of which the ‘‘mass over momentum ratio’’ cuts were ineffective.

VI. ENERGY LOSS

Figures 5 and 6 are plots of the energy loss expected in TOF1 and TOF2 respectively for various particles as a function of their apparent momentum. The true momentum of doubly ionized particles will be twice what appears on the

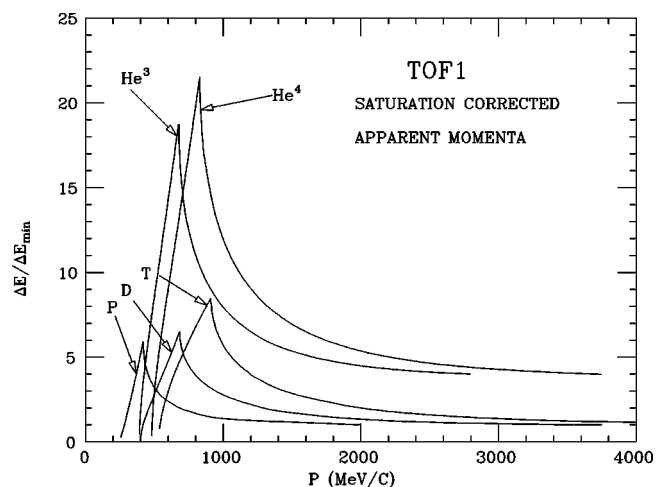


FIG. 5. Light output from TOF1 as a function of apparent momentum, assuming charge is 1e, for various particles. Curves are corrected for light saturation in the scintillator material.

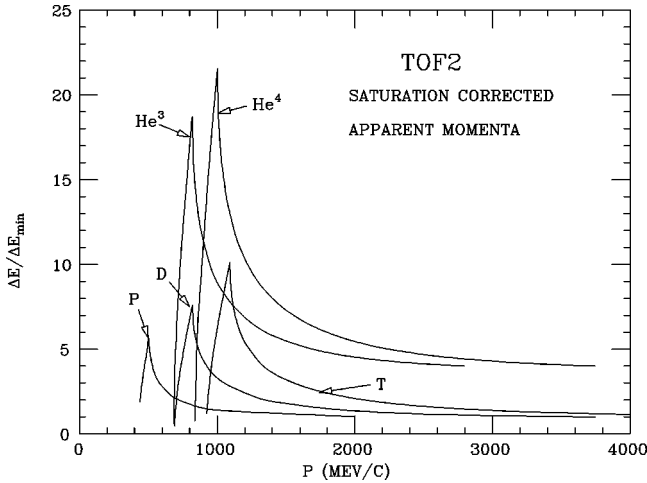


FIG. 6. Light output from TOF2 as a function of apparent momentum, assuming charge is $1e$, for various particles. Curves are corrected for light saturation in the scintillator material.

abscissa of these figures. Since we have no *a priori* way of knowing the charge of a given track, we always work with the apparent momentum which is calculated assuming the magnitude of the charge is $1e$. The vertical scale is in multiples of the energy loss expected from the passage of a minimum ionizing pion.

These energy loss curves were corrected for saturation effects in the scintillator for massive low energy particles. We have made use of data supplied by Bicron [7] for plastic scintillators. These data give the ratio of light output from stopping heavy particles to stopping electrons as a function of momentum. For particles with momentum greater than that necessary to penetrate a TOF scintillator, we approximate saturation effects using the relation [8]

$$dL/dx = A (dE/dx) / [1 + k (dE/dx)] \quad (2)$$

where dL/dx is the light output per centimeter of scintillator and dE/dx is the energy loss per centimeter. The constant A is determined by minimum ionization expectations at momentum $p = 2mc$. The constant k is fixed by Bicron saturation data for particles with just enough momentum to penetrate a TOF counter thickness. We have checked the light yield curve for TOF1 in Fig. 5 with proton data and found good agreement. Since the anode signals from TOF2 phototubes could not be corrected for space charge effects with a dynode 9 signal, we used the proton curve of Fig. 6 to obtain an average correction for these space charge effects. The overall reliability of these curves is important for the remaining analysis.

VII. CUTS ON THE DATA

Examination of Fig. 5 and Fig. 6 will reveal the difficulty to be encountered in identifying the light nuclei. The most restrictive problem is that some ADC's will saturate for light output corresponding to ΔE greater than 6 times minimum ionization. Without the ΔE information this experiment can measure only the ratio of mass to charge (m/q). If one plots

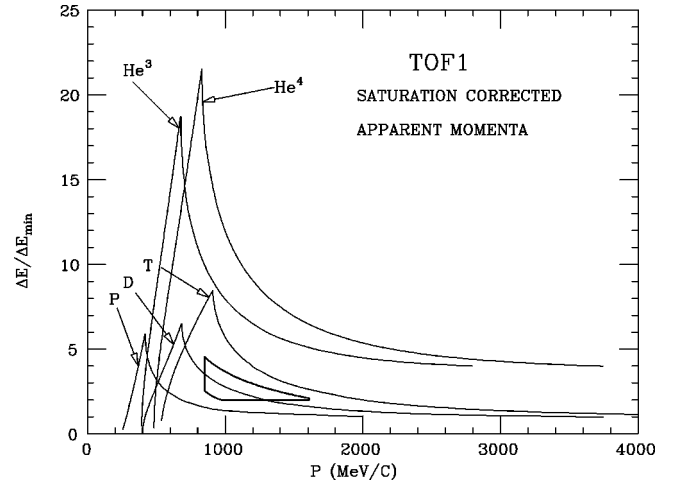


FIG. 7. The box outline on the deuterium curve defines an area in which deuterium event candidates must lie.

the number of events vs m/q , both ${}^4\text{He}$ and deuterium would peak at the same place, as would many other nuclei. We will assume that nuclei heavier than ${}^4\text{He}$ are produced so rarely that they are not observed in this experiment. Then we will search in a range of apparent momentum where our measurements of pulse height can distinguish between a charge of $1e$ and greater charges. To obtain a cross section we must correct for data that is possibly excluded from our search range.

Figure 7 shows cuts applied to produce a search region for deuterium when using TOF1. The box on the deuterium curve outlines an area in which events must appear to be considered as deuterium candidates. A similar box with the same momentum limits was chosen for TOF2.

VIII. LUMINOSITY

During the experiment accelerator operators studied the beam luminosity by periodically monitoring scattering from a flying wire passed through the beam bunches [9]. These luminosity results were recorded along with our other data. Once these results were well enough understood, they were used to calculate the luminosity for the crossing bunches at our intersection. Well-understood luminosity measurements could be obtained for approximately 2/3 of our data. The luminosity for the remaining data was estimated by comparing the flux of protons in the spectrometer for measured and unmeasured luminosities. To make the flux comparisons, each observed proton had to be weighted by the prescale factor for the event that contained it. The integrated luminosity for the live time of the complete data sample was $\int \mathcal{L} dt = 12.48 \pm 1.84 \text{ nb}^{-1}$.

IX. DEUTERON CROSS SECTION

In general we determine particle masses using TOF1 and TOF2 measurements separately. A scatter plot of m_1^2 versus m_2^2 for an event has most of the points lying along the diagonal $m_1^2 = m_2^2$. Events which do not have points along the diagonal are usually well removed from the diagonal and are

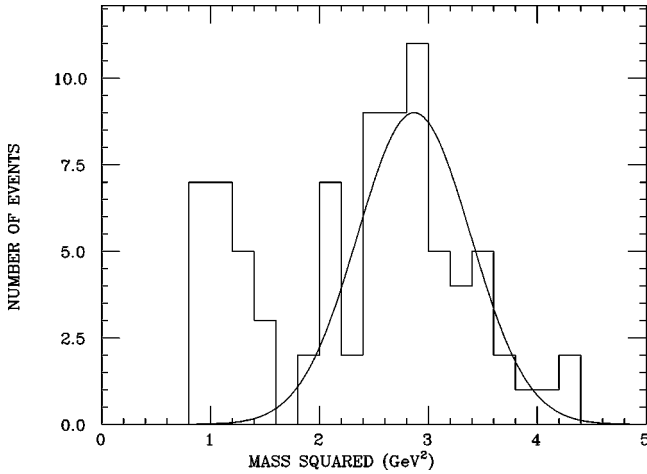


FIG. 8. A plot of the mass squared distribution based on the average of TOF1 and TOF2 measurements for both negative and positive particles. dE/dx and momentum cuts were used to favor deuteron selection. The curve shows the expected mass resolution for deuterons and is not a fit to data.

easily eliminated by cuts. Mass peaks are best resolved from one another by projecting the remaining scatter plot points on the diagonal axis. Since data points lie close to the diagonal axis, this procedure essentially plots points versus the average mass squared of the two measurements. Figure 8 shows such a projection of data versus average mass squared after applying the previously described momentum and ΔE cuts to select deuterium. Both positive and negative tracks are included in the plot to increase statistics.

One can see a remnant of protons near a mass squared of 1.0 $(\text{GeV}/c)^2$. The expected mass resolution for deuterons plotted in Fig. 8 was estimated by a Monte Carlo simulation using the results of measuring error studies on the more plentiful lighter particles. It is shown here to convey the expected mass resolution for deuterons and is not a fit to the data. The center of the curve is placed at a mass-squared value that corresponds to a deuterium mass about 8% lower than the nominal value. We attribute the apparent mass shift of the data to a time-walk correction made to time to digital converter (TDC) times. This correction algorithm was optimized using lighter ionizing particles. An overcorrection for heavily ionizing particles would give systematically smaller mass values.

The events plotted under the curve in Fig. 8 are used to obtain the deuteron production cross sections, but the points plotted are not weighted by the trigger prescale factors that must be used for cross section calculations. Trigger prescale factors range from 1 to 26, and if used in plotting with low statistics data samples, produce deceptively irregular histograms.

In the raw data we find 38 deuteron events and 19 anti-deuteron events. Each individual event was weighted by its associated prescale factor and further corrected for a cut which eliminated events with multiple tracks in a TOF counter or events with hits in scintillators adjacent to the deuteron candidate. Corrections were made for absorption in 0.15 interaction lengths of spectrometer material based on

cross sections from the Particle Data Group [10]. The absorption correction factor applied to deuterons was 1.11 and that applied to antideuterons was 1.66.

A Monte Carlo simulation of the deuteron acceptance which assumed a flat rapidity distribution and a momentum spectrum (discussed below) agreed well with the observed deuteron rapidity distribution. The results of the Monte Carlo simulation were then used to make geometrical acceptance corrections. Since tracks were not used in the deuteron search unless all 3 planes of the vertex chamber contributed data points, this required a further correction of 20%.

Invariant differential cross sections for deuteron production may be calculated without relying on details of the deuteron momentum distribution. For rapidity $y=0$ and average momentum $p=1.225 \text{ GeV}/c$, these are

$$\begin{aligned} d^3\sigma(d^+)/d^3p/E &= (1/2\pi)d^2\sigma/dy p_T dp_T \\ &= 149 \pm 33 \text{ nb/GeV}^2, \end{aligned} \quad (3)$$

$$\begin{aligned} d^3\sigma(d^-)/d^3p/E &= (1/2\pi)d^2\sigma/dy p_T dp_T \\ &= 103 \pm 28 \text{ nb/GeV}^2. \end{aligned} \quad (4)$$

A much more useful cross section for comparison with the central production of other particles would be $d\sigma/dy|_{y=0}$, where the transverse momentum dependence of the invariant cross section has been integrated out. Since we accepted only a portion of the momentum spectrum, it becomes necessary to assume a momentum spectrum for the deuterons in order to correct for the unobserved deuterons. We have investigated two models for this momentum dependence.

The first model is a mass dependent, relativistic thermal model [11] of the form

$$dN/dp = Ap \exp(-\sqrt{p^2+m^2}/T) \quad (5)$$

where m is the mass of the particle, and p is its transverse momentum. A value of $T=253 \text{ MeV}$ gives a very acceptable fit to the antiproton momentum spectrum in this experiment. The dot-dashed curve in Fig. 9 is a plot of this curve for the deuteron mass.

The coalescence model [2] has successfully described momentum distributions for produced nuclei by constructing a product distribution from the momentum distributions of the constituents, evaluating each constituent momentum at p/N , where N is the number of constituents. We find a good fit to our proton momentum spectrum can be obtained with an exponential in transverse momentum. This suggests that for deuterons we use the function

$$dN/dp = A\{(p/2)\exp[-b(p/2)]\}^2, \quad (6)$$

where b is obtained from fitting the proton spectrum. This function is plotted as the solid curve in Fig. 9.

It is interesting to note that even a high statistics version of this experiment would have difficulty distinguishing the coalescence model and the relativistic thermal model. Both models predict a momentum acceptance of 39% for collecting deuterons in our transverse momentum interval $0.85 < p < 1.6 \text{ GeV}/c$.

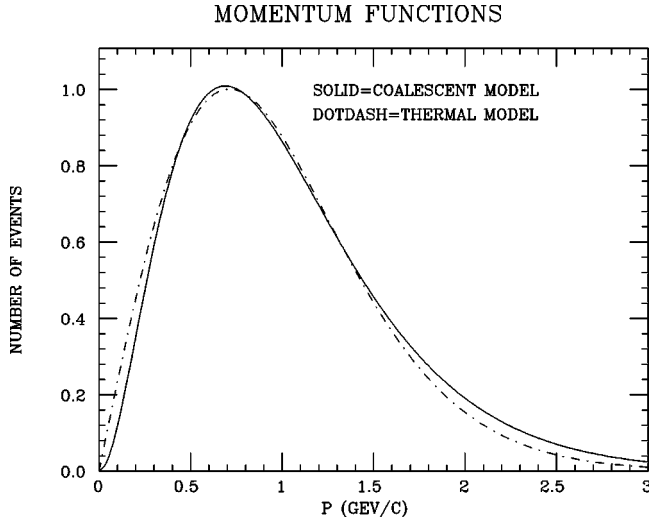


FIG. 9. Two models for the deuteron momentum distribution. Solid curve: distribution is the square of the measured proton momentum distribution at half the deuteron momentum as used in the coalescence model. Dot-dashed curve: distribution is a thermal model using the deuteron transverse mass in the Boltzman factor.

The calculated cross sections per unit rapidity at $y=0$ are

$$d\sigma(d^+)/dy|_{y=0} = 2.18 \pm 0.48 \mu\text{b} \quad (7)$$

and

$$d\sigma(d^-)/dy|_{y=0} = 1.58 \pm 0.43 \mu\text{b}. \quad (8)$$

Cross section errors are determined almost equally by two effects: the small number of candidate events and the uncertainty in absolute integrated luminosity. The two cross sections are equal within errors. The systematic uncertainty introduced by the assumption of a deuteron momentum distribution has not been included in the errors, but the success of the coalescence model in other situations suggests that this does not make a major contribution to the error.

An independent measurement of proton or anti-proton production gives [12]

$$d\sigma(p^-)/dy|_{y=0} = d\sigma(p^+)/dy|_{y=0} = (4.34 \pm 0.65) \text{ mb}. \quad (9)$$

The ratio of deuteron to proton production in central collisions is thus $d^+/p^+ = (5.0 \pm 1.0) \times 10^{-4}$. The luminosity error cancels in calculating this ratio.

X. ASSOCIATED CHARGED MULTIPLICITY

A charged multiplicity N_c was measured for each event by barrel and endcap hodoscopes. Hodoscope elements covered the pseudorapidity range $\eta < |3.25|$. A correction was made to the number of scintillator hits to account for the finite size of the scintillator elements [13].

The average of the charged multiplicity for events with an associated deuteron in the spectrometer arm was $\langle N_c \rangle = 67 \pm 21$. This value of $\langle N_c \rangle$ is plotted in Fig. 10. The average charged multiplicity for events with a deuteron in the spec-

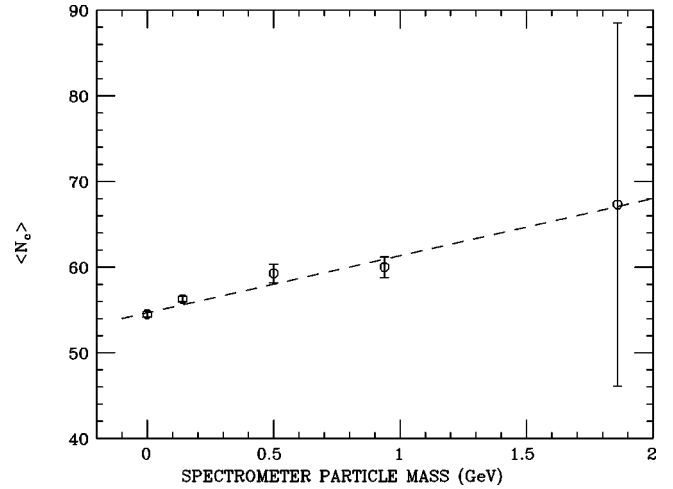


FIG. 10. Average charged multiplicity in the pseudorapidity interval $\eta < |3.25|$ vs particle mass found in the spectrometer arm near 90° . Since minimum bias triggers most frequently had no spectrometer particle, this multiplicity is plotted at zero mass.

trometer arm had to be computed with data collected for the entire experiment using a large variety of triggers and prescale factors. Low multiplicity events were heavily prescaled. A few of these events dominated the error calculation for average multiplicity.

Also plotted for comparison is the average charged multiplicity in the same pseudo-rapidity interval when pions, kaons, or protons are found in the spectrometer arm. Adequate statistics for these particle types could be obtained from a few short data runs with unbiased triggers.

There may be a slight increase of multiplicity with particle mass as indicated by the dashed line. Deuteron production could be consistent with this increase, but it does not show any sign of being remarkably different from the general trend.

XI. TRITIUM

A search was made for a tritium signal using momentum and dE/dx cuts that should strongly suppress background from other sources. The dashed box in Fig. 11 shows an area selected for the TOF1 counter. A similar box was selected for the TOF2 counter. Eight events, insufficient to form a convincing mass peak, were found in the mass interval expected for tritium as predicted by our mass resolution function. There were no events at mass values higher than the tritium mass interval. Seven other events were discarded. Some of these had three inconsistent mass values and some had good proton mass values together with large enough Landau fluctuations to pass ΔE cuts for TOF1 and TOF2.

If we assume these candidate events were all positively charged tritium, we can estimate a cross section at $y=0$ using the approach outlined for deuterium earlier. In this case the momentum spectrum given by the coalescence model differs somewhat from that given by a thermal model, and the resulting cross sections disagree by 20%. An average of these two values gives a cross section for tritium at $y=0$ of

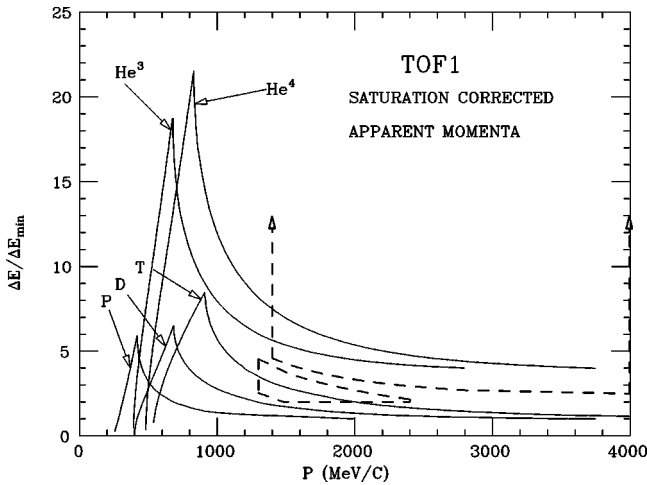


FIG. 11. Dashed regions indicate areas used in searching for tritium and helium signals.

$$d\sigma(t^+)/dy|_{y=0} = 0.83 \pm 0.32 \mu\text{b}, \quad (10)$$

where the error includes systematic effects. The corresponding invariant cross section for tritium production at $y=0$ and $p_T=1.5 \text{ GeV}/c$ is

$$(1/2\pi)d^2\sigma(t^+)/dy p_T dp_T = 35 \pm 13 \text{ nb/GeV}^2. \quad (11)$$

One expects antitritium to be heavily absorbed in the material of the spectrometer. No attempt was made to calculate a cross section for it.

XII. HELIUM

Figure 11 shows a dashed open box which outlines the cuts used with TOF1 to search for a signal from ${}^4\text{He}$ and ${}^3\text{He}$ events. A similar cut was used simultaneously for TOF2. Although events with any large value of dE/dx were accepted, most counters or TDC's saturated a little above 6 times minimum. This saturation prevented us from searching in the momentum region where the greatest potential existed for separating helium from the nuclei with unit charge. The momentum acceptance is expected to be small in the region outlined, 4% according to the coalescence model and 1.5% according to the thermal model.

There were no acceptable events found in the mass regions expected for either isotope of positive helium. Our method of calculating cross sections requires us to observe an event in order to know its prescale factor. Using the average prescale factor observed for deuterium events, we can nevertheless estimate helium cross sections that would have been implied by the observation of one event using a coalescence momentum model and a thermal momentum model respectively. One ${}^3\text{He}$ event would imply $d\sigma/dy|_{y=0} \approx 500 \text{ nb}$ or $d\sigma/dy|_{y=0} \approx 1400 \text{ nb}$. One ${}^4\text{He}$ event would imply $d\sigma/dy|_{y=0} = 150 \text{ nb}$ or $d\sigma/dy|_{y=0} = 700 \text{ nb}$.

XIII. BIG BANG COMPARISON

The large disparity between nuclear binding energies and multiparticle collision temperatures suggests there is little

connection between the big bang model of nucleosynthesis and the nuclear production we observe in elementary particle collisions. However, the fact that the d/p ratio produced in high energy collisions is larger than that predicted by big bang nucleosynthesis could potentially affect conclusions about measurements of this ratio in interstellar gas clouds. This is discussed below.

The big bang model makes a prediction of the baryon density in the universe that is simply related to its prediction of the relative primordial abundances of the light elements H, D, ${}^3\text{He}$, ${}^4\text{He}$, and ${}^7\text{Li}$ [14]. In this model the ratio of deuterium to hydrogen is the most sensitive predictor of baryon density in the universe and thus gives information on the possible closure of the universe.

Interstellar measurements of the atomic D/H ratio are generally taken to be *lower limits* for the primordial ratio, since nuclear reactions in the evolution of stars are expected to deplete the relative amount of deuterium [15]. Measurements on the absorption of quasar light in low metal hydrogen clouds have given D/H values between 2.3×10^{-5} and 5.7×10^{-4} [16–18]. Low metal content makes these clouds candidates for primordial hydrogen that has not undergone stellar evolution. The lower values for D/H imply a higher baryon density for the universe and seem to be theoretically favored [14].

Because the d/p production ratio observed in this experiment is approximately an order of magnitude greater than the currently favored primordial D/H ratio, irradiation of primordial gas clouds by cosmic rays or other high energy particle fluxes could have in principle increased the D/H ratio over long periods of time. For cosmic ray fluxes the size of those in our neighborhood of the universe the cross sections we measure for deuteron pair production are too small by many orders of magnitude to produce a significant increase in the D/H ratio of hydrogen gas clouds, even if these reactions were to be integrated over the age of the universe.

XIV. SUMMARY

We have observed signals for centrally produced deuterium and antideuterium in $p\bar{p}$ collisions at $\sqrt{s}=1.8 \text{ TeV}$ and have calculated absolute cross sections for the production rates. We use these cross sections together with those for producing protons and antiprotons in the same rapidity interval to calculate a d/p production ratio for high energy hadron collisions. Some evidence was found for tritium production, and a cross section estimate was made. No helium isotopes were observed, but the sensitivity of the apparatus was not optimum for such a search.

ACKNOWLEDGMENTS

We are indebted to the Fermilab staff. Valuable contributions to the data processing were made at times by S. Tufte, J. Bevic, X. Chen, and D. Thurs. We wish to thank N. Gelfand and C. Grosso-Pilcher for assistance in understanding the results on Tevatron luminosity data. F. Scherb was most helpful in providing recent astronomical reports.

- [1] D.E. Dorfan *et al.*, Phys. Rev. Lett. **14**, 1003 (1965).
- [2] A.Z. Mekjian, Phys. Rev. Lett. **38**, 640 (1977); F.S. Rotondo, Phys. Rev. D **47**, 3871 (1993).
- [3] H. Albrecht *et al.*, Phys. Lett. B **236**, 102 (1990).
- [4] T. Alexopoulos *et al.*, Phys. Rev. D **48**, 984 (1993); T. Alexopoulos *et al.*, *ibid.* **48**, 1931 (1993).
- [5] S. Banerjee *et al.*, Nucl. Instrum. Methods Phys. Res. A **269**, 121 (1988).
- [6] C. Hojvat *et al.*, Nucl. Instrum. Methods Phys. Res. A **337**, 306 (1994).
- [7] Bicon Corporation, Newbury, OH, a susidiary of Saint-Gobain Industrial Ceramics, Inc.
- [8] G.D. Badhwar *et al.*, Nucl. Instrum. Methods **57**, 116 (1967).
- [9] N. Gelfand, "Computation of the Tevatron Luminosity Using Measured Machine Parameters," Report No. Fermilab-FN-538, 1990.
- [10] Particle Data Group, R. M. Barnett *et al.*, Phys. Rev. D **54**, 1 (1996).
- [11] S.R. de Groot, W.A. van Leeuwen, and Ch. G. van Weert, *Relativistic Kinetic Theory* (North-Holland, Amsterdam, 1980).
- [12] K. Gulbrandsen, Senior thesis, University of Wisconsin-Madison, 1998.
- [13] T. Alexopoulos *et al.*, Phys. Rev. Lett. **60**, 1622 (1988).
- [14] David M. Schramm and Michael S. Turner, Nature (London) **381**, 193 (1996).
- [15] R. I. Epstein, J. M. Lattimer, and D. N. Schramm, Nature (London) **263**, 198 (1976).
- [16] D. Tytler, X.-M. Fan, and S. Burles, Nature (London) **381**, 207 (1996); D. Tytler *et al.*, Astron. J. **117**, 63 (1999).
- [17] A. Songaila *et al.*, Nature (London) **368**, 599 (1994).
- [18] R.F. Carswell *et al.*, Mon. Not. R. Astron. Soc. **268**, L1 (1994).